

# The Effect of a Printed Gap Waveguide Antenna at 60 GHz on the Human Body

<sup>1</sup>Electrical Engineering Department, Higher Technological Institute, HTI, 10th of Ramadan city, Egypt.

<sup>2</sup>Department of Electrical Engineering, Assiut University, Egypt.

<sup>3</sup>Department of Electrical and Computer Engineering, Concordia University, Montréal, Quebec, Canada.

<sup>4</sup>Communications and Electronics Engineering Department, Faculty of Engineering, Minia University, Minia, Egypt.

<sup>5</sup>Communications Department, Information and Engineering Technology, German University in Cairo, Egypt.

\* corresponding author E-mail: [haitham.ezzat@hti.edu.eg](mailto:haitham.ezzat@hti.edu.eg)

## ABSTRACT

Millimetre-wave (mm-Wave) bands are becoming increasingly relevant for modern communication standards due to their large bandwidth and enhanced security. This development in communications standards has inspired the emergence of innovative antenna configurations within these bands. Moreover, a growing concern over the possible adverse consequences of mm-Wave frequency exposure on human health motivates investigations into mm-Wave frequency's impacts on the human body. This paper investigates the impact of a Printed Gap Waveguide (PGW) antenna on the human body at 60 GHz. A Magneto-Electric (ME) dipole antenna with broadband operation and identical radiation characteristics in the mm-Wave band is proposed. PGW technology is utilized to implement a ME dipole antenna for studying human body exposure to 60 GHz Electromagnetic (EM) radiation. ME-dipole elements have been developed and examined, and EM exposure is calculated in terms of Specific Absorption Rate (SAR). The antenna is made up of a cross-shaped ME-dipole that is supported by an Artificial Magnetic Conductor (AMC) side wall cavity. The antenna with the proposed design achieves 23.4% relative impedance bandwidth at 60 GHz over the entire operating frequency range. Simulations were performed to investigate and validate the performance of the structure using Computer Simulation Technology (CST) and a high-frequency structure simulator (ANSYS HFSS). On the basis of the presented results, there is a clear advantage in evaluating the Specific Absorption Rate (SAR) according to this state-of-the-art guiding structure and meeting the global standards.

**Keywords:** Millimetre-Wave (mm-Wave) Communications, Head Phantom, Specific Absorption Rate (SAR), Magneto-Electric (ME) Dipole, Printed Gap Waveguide (PGW).

## I. INTRODUCTION

Wireless communication networks have made it possible for billions of people to be linked to the internet so that they can enjoy the benefits of today's digital economy [1]. In addition, the expansion of bandwidth-hungry wireless applications has driven demand for technologies that can support larger bandwidths. Furthermore, the current level of saturation in the microwave spectrum emphasizes attention to new frequency ranges. As a result, the emergence of bands with broad bandwidth capable of meeting the anticipated high data rate for handling ultra-high-speed applications was required [2]-[4]. Therefore, the utilization of mm-Wave frequency bands has been considered a vital step towards the realization of future wireless communication systems [5]. The unlicensed 60 GHz range (from 57 to 66 GHz) specifically has a considerable potential for high-data-rate wireless communications [6], [7].

Furthermore, the 60 GHz band can be provided to promote the ISM band to higher frequencies in order to satisfy the data rate demands of next-generation wireless communication systems [8]. Besides the high data rates that can be reached in this spectrum, energy propagation in the 60

GHz band has specific characteristics that provide for a multitude of other advantages, such as superb immunity to interference and a high level of frequency reuse [9], [10]. Although the 60 GHz band provides additional spectrum, excessive signal attenuation is going to be a significant hurdle to 60 GHz communications [11]. This can be attributed to the fact that the atmospheric absorption at 60 GHz has a significant impact on transmission distances [12]. Consequently, a high gain broadband antenna is considered a remedy for such diminution, which may be accomplished by utilizing proper feeding networks developed using different techniques [13]-[15]. It might be challenging to design such antennas in order to achieve acceptable performance in terms of gain and efficiency while minimizing complexity. Therefore, there is a great demand for wide-band and compact antennas suitable for a wide range of mm-Wave communication systems. In addition to providing superior electrical characteristics such as minimal cross-

polarization, low back-lobe radiation, and stable gain all over the whole bandwidth.

Based on this concept, a wide-band complementary antenna known as the ME dipole was developed [16]. The ME dipole antenna has recently received significance due to its beneficial characteristics such as a wide impedance bandwidth, high front to back ratio, and identical radiation patterns. The principle behind a ME dipole antenna is to simultaneously excite both an electric dipole and a magnetic dipole, resulting in identical H- and E-planes and stable radiation patterns [17]. A wide range of research has been conducted for the development of ME dipole antenna structures with complementary sources of an electric and a magnetic dipole in the 60 GHz band [18]-[20]. The antenna system's feeding networks are different based on the guiding structure employed.

Microstrip line technology has been reported as being significantly lossy at mm-Wave bands and having large radiation losses, which is mainly the reason for antenna system efficiency degradation [21], [22]. In addition, substrate-integrated waveguide (SIW) technology improves isolation; however, at mm-Wave, the dielectric losses subject the system to degradation, which incurs additional costs and complexity [23], [24]. Hollow metal waveguides provide the lowest insertion losses, but they must be implemented by carving grooves into the metal plate before covering it with another metal plate. This should be performed in order to guarantee electrical connections and precise sealing, which is challenging and costly in mm-Wave applications. Considering typical millimetre-wave technologies' limitations, new guiding structures are required to address these shortcomings and provide low-loss circuits at mm-Wave. Gap waveguide (GW) technology has demonstrated multiple benefits in millimetre-wave antennas, alongside other various components. Gap waveguide technology was launched in 2009 as a high-frequency new alternative to hollow waveguides, microstrip lines, SIW, and other traditional guiding structures [25]- [27]. GWs are more cost-effective and planar compared to hollow waveguides, especially for high frequencies such as millimetre waves. The latter is due to the fact that there are no mechanical joints through which electric currents must float. On the other hand, GWs have lower losses than microstrip lines, and they are completely self-shielded, eliminating additional packaging requirements, unlike microstrip circuits, which suffer from substantial packaging problems. In addition, SIW structures suffer from losses due to the presence of the substrate and the metallization via holes, which is an expensive complication.

The basic concept of GW resembles that of a PEC-PMC parallel plate waveguide. No propagation emerges between PEC-PMC plates when the gap separation is less than  $\lambda/4$  [28]. GWs are realized in a narrow gap between two parallel metal plates, utilizing a texturing or multilayer structure. A periodic PEC bed of pin texture has been utilized to form the PMC plate. A guiding wave mode can be generated by adding a ridge or groove between the pins [29]-[34]. The waves can follow the metal ridge within the textured surface. A high surface impedance (PMC) at both sides of the ridge prevents propagation in any other direction. In this way, PEC-PMC parallel plates are employed, resulting in a proper frequency stopband [35], [37].

As a result, cavity resonances cannot be observed within this operating range.

Furthermore, GW construction prevents wave leakage because there is no electric contact between the metal plates. Moreover, the PGW is proposed as a new promising guiding medium in the mm-Wave range due to recently reported advantages such as low loss, self-packaging, and quasi-TEM propagating mode [38]-[41]. PGW is a lightweight and inexpensive approach that has recently been employed for enhancing mm-Wave antenna performance. Therefore, the ME dipole antenna based on PGW technology at 60 GHz is presented.

Since any wireless device must include antennas or antenna arrays that are always close to the customer's body, the extreme attachment of people to cell devices can lead to long-lasting exposure to EM radiation [42],[43]. So, EM exposure to wireless devices is to be firmly regulated globally to ensure the safety of consumers [44]. The Specific Absorption Rate (SAR) is considered a major parameter to define the safety limits, which is defined as the EM energy rate absorbed by biological tissue. SAR gives a convenient means of measuring the RF exposure attributes of wireless devices to ensure that they comply with the safety standards laid down by the U.S. Federal Communications Commission (FCC).

The characteristics of the 60 GHz band are unique and enable many advantages, such as excellent immunity to interference, high protection, and frequency reuse [45]. Additionally, high data rates can be achieved in this spectrum. High-frequency emissions at 60 GHz can be absorbed by the moisture in the human body and hence do not penetrate beyond the skin's outer layers. So, the 60 GHz systems present the solution of compromising between performance and safety over other RF communication systems.

The SAR limit for wireless devices is 1.6 W/kg according to the guidelines of the Institute of Electrical and Electronic Engineers (IEEE) and FCC [46], averaged over 1 gramme of tissue. While the SAR limit is 2.0 W/kg according to the guidelines of the International Commission on Non-Ionizing Radiation Protection (ICNIRP) [47], it averages over 10 grammes of tissue. As all wireless devices must be supplied with SAR values, there is strong compliance with the listed guidelines requirements for efficient SAR antenna implementation theories and techniques.

Recent studies have discussed the SAR evaluation [48]-[51]. Further research investigated the SAR calculations at 60 GHz., providing various antennas working in this promising band. Single and layered human tissues with a microstrip patch antenna interaction at mm-Wave frequencies of 28, 40, and 60 GHz are proposed along with an EM radiation study [52]. A model of human tissue is exposed to a radiating source by increasing the antenna radiating power from 20 dBm to 24 dBm, where the SAR is evaluated. This study highlighted that at 60 GHz, the evaluated SAR is higher than the other bands, showing that the SAR value increases with frequency. Another study discussed the SAR distribution analysis for a substrate-integrated waveguide (SIW)-based slot antenna [53]. The SAR distributions in homogeneous phantom model due to SIW-based antenna are computed at 60 GHz. The measured SAR at 60 GHz

with transmitting powers of 1, 10, and 100mW are demonstrated in this investigation. EM exposure was observed in terms of SAR on 3D human tissue models representing two body parts, the head and anterior thighs, at 60 GHz. Another method for calculating SAR in the human head is EM modelling of the human head with a dipole excitation at 60 GHz [54].

Based on the literature, evaluated SAR levels at 60 GHz in tissues have a variation of 0.885 to  $7e+12$  with an approximately 5 mm distance between tissues and the source. On the other hand, the risk of significant radiation losses is a possible downside of guiding structures such as microstrip and SIW that have a significant impact on the SAR value. This promotes other innovative guiding structures, such as the PGW, to meet the growing interest in mm-Wave communication systems. The proposed PGW antenna has been demonstrated with considerable safety limits to be a good candidate for 60-GHz applications. In the following sections, the antenna configuration, design guidelines, and performance of the proposed antenna, including gain enhancement, are presented. Afterwards, a modelling approach incorporating simplification criteria was described, and SAR results calculated on the simplified human model were demonstrated.

## II. Magneto-Electric Dipole Antenna Design

### a. Antenna Configuration

The proposed antenna geometry is depicted in Fig. 1, which consists of three Rogers RT6002 substrates with a dielectric constant of  $\epsilon_r = 2.94$  and a thickness of 0.762 mm. In contrast to [55], which only uses one dipole, four adjacent square metallic patches representing electric dipoles are printed on the top of the substrate. Each patch is connected to the substrate ground via a series of five metallic plated via holes set around the patch's inner corner. Such a design facilitates the antenna to be used in the mm-Wave spectrum instead of using inverted-L wires [56]. While a cross-shaped aperture extends from the top substrate ground to the patch forming the magnetic dipoles. This cross-shaped aperture consists of two rectangular apertures, representing vertical and horizontal magnetic dipoles, respectively.

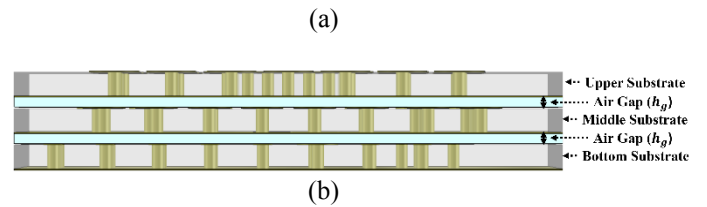
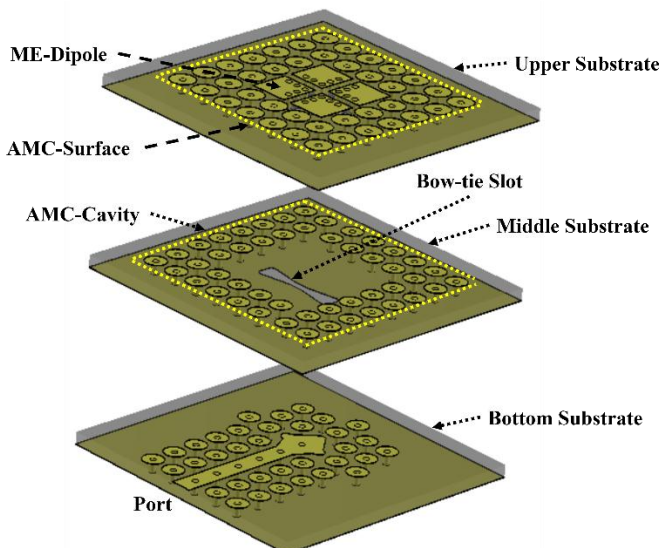
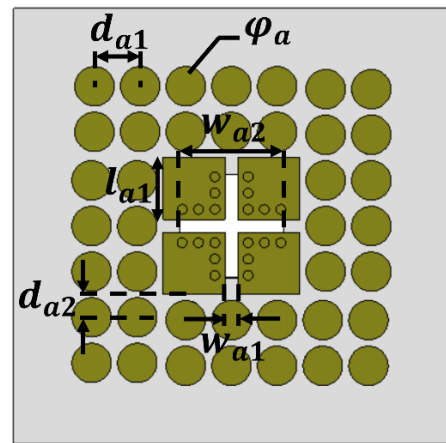
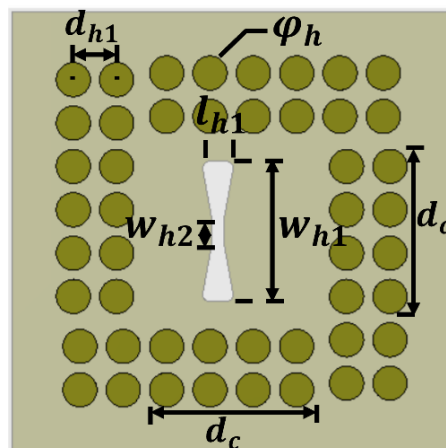


Fig. 1. (a) 3D view of the proposed antenna geometry. (b) Side view.

This cross-shaped groove acts as a feeding aperture, excited by a PGW line printed on the bottom substrate through a bow-tie slot. This structure differs slightly from the reported L-probe feed ME dipole antenna. In this study, an electromagnetic band gap (EBG) mushroom-shaped structure forming an AMC cavity is implemented for antenna excitation. In the upcoming sections, it is demonstrated to be effective in tuning the impedance matching and enhancing the gain of the proposed design.



(a)



(b)

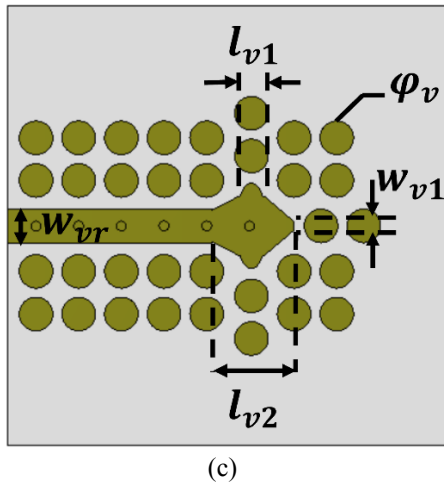


Fig. 2. The proposed antenna layers top views (a) Upper substrate. (b) Middle substrate with a bow-tie slot etched on the ground layer. (c) Bottom substrate.

**b. Design Guideline**

The proposed work employs a ME-dipole antenna that achieves stable radiation characteristics across a broad operational frequency spectrum. The electric dipoles are formed with a pair of patches mounted on the top substrate surface, as illustrated in Fig. 2(a), while the magnetic dipoles have been represented by the apertures between the metallic patches. In comparison with a conventional ME dipole with an L-shaped probe, it is found that a coupling aperture makes it challenging to achieve good impedance matching. Therefore, a square AMC side walls cavity is utilized for antenna excitation. This cavity is excited by a PGW line mounted in the bottom substrate with an input port. Fig. 2(b) demonstrates the mushroom-shaped EBG structure that forms the AMC walls. Moreover, the input power from the port is directed to the cavity via a symmetrical end-launch PGW configuration, as illustrated in Fig. 2(b). To properly couple the input power to the ME dipole antenna with minimal reflection, the cavity is adopted. An etched Bow-tie slot on the bottom ground of the middle substrate couples the input signal from the input port. For an adequate coupling and impedance bandwidth, the feeding PGW line in the bottom layer is terminated with a matching stub. The PGW line with a matching stub feeding this slot as shown in Fig. 2(c). The feeding PGW line has been designed with a bow-tie slot to achieve deep matching level and provide a broad impedance bandwidth of the antenna. The slot is quite moved from the center in order to provide a wide impedance matching bandwidth.

A PGW line design and EBG unit cell characteristics and dimensions with a bandgap controlled by a mushroom-shaped EBG structure are discussed in a number of studies [37]-[39], [57]-[59]. The dispersion diagram for the row of unit cells associated with the designed PGW section is depicted in Fig. 3. The air gap for the proposed PGW line has been configured to  $h_g = 0.254\text{mm}$ , whereas the conducting layer thickness is set to be  $0.035\text{mm}$ . The diagram was calculated using the Computer Simulation Technology (CST) Eigen mode solver, and it indicates that a bandgap occurs between 24 and 70 GHz, where the quasi-TEM mode is propagating. The detailed proper dimen-

sions of the presented ME-dipole antenna and the PGW structures are provided in Table. 1.

Table 1. Dimensions of the presented ME dipole antenna (in mm).

Parameter	$d_{a1}$	$d_{a2}$	$w_{a1}$	$w_{a2}$	$w_{v1}$	$l_{v1}$
Value	0.9	0.5	0.25	2.05	0.2	0.45
Parameter	$l_{a1}$	$\phi_a$	$d_{h1}$	$w_{h1}$	$\phi_h$	$l_{v2}$
Value	1.25	0.8	0.85	2.8	0.65	1.6
Parameter	$w_{h2}$	$l_{h1}$	$d_c$	$w_{vr}$	$\phi_v$	$h$
Value	0.5	0.3	3.95	0.685	0.65	0.762

The performance of the antenna at the operating frequency of 60 GHz is shown in Fig. 4, where a matching level less than -15 dB is achieved from 56 to 66 GHz. Moreover, the gain has been demonstrated which shows more than 9 dBi. The reflection coefficient has been compared with another simulator HFSS to validate the performance. Furthermore, the simulated 3D radiation patterns in both the E-plane and the H-plane for different operational frequencies are depicted in Fig. 5.

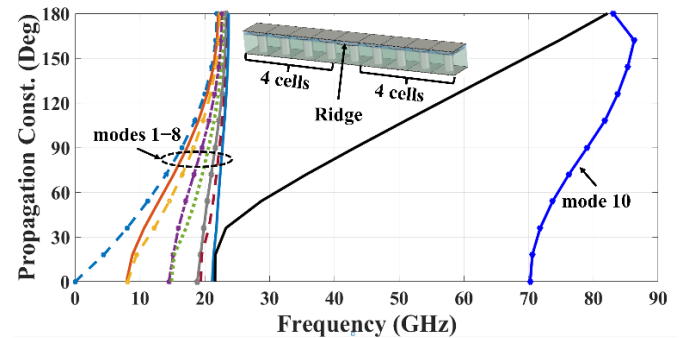


Fig. 3. Dispersion diagram of PGW row of unit cells.

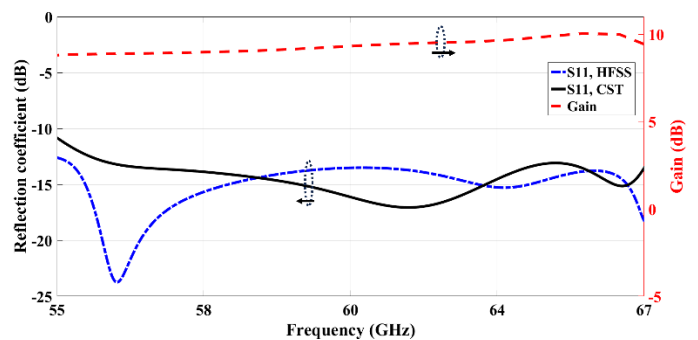


Fig. 4. The Reflection Coefficient of The Proposed Antenna.

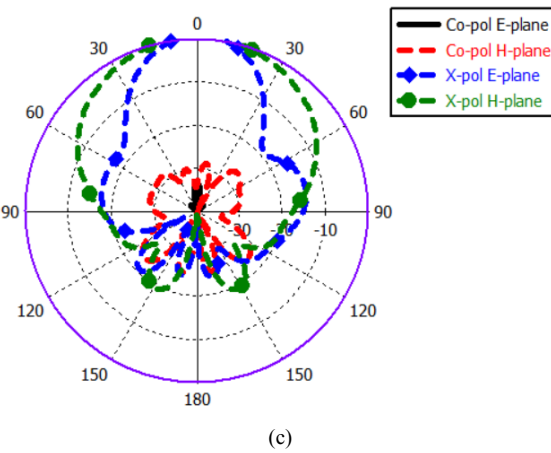
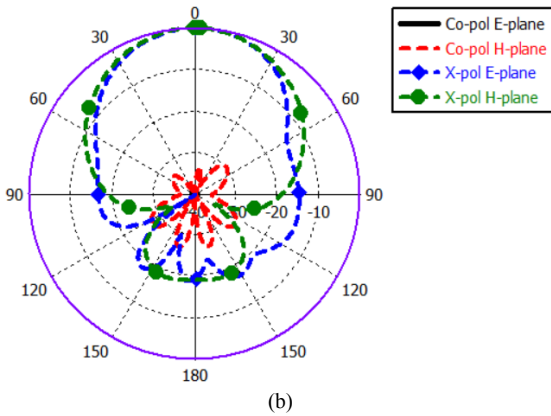
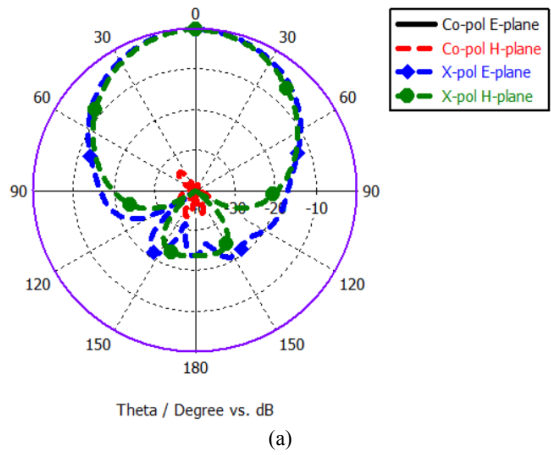


Fig. 5. The proposed antenna radiation pattern at 60 GHz..(a) 56 GHz. (b) 60 GHz. (c) 66 GHz.

**c. Gain Enhancement of The Presented Antenna**

An AMC surface can be deployed to surround ME-dipole antennas to enhance the gain of the presented antenna, as shown in Fig. 2(a). The literature introduces various techniques for realizing the AMC, with the deployment of a mushroom form representing the most effective and simple technique with a wide operating bandwidth. The mushroom-shaped EBG unit cell in the suggested design has been chosen to achieve adequate matching as well as better performance over the whole bandwidth. The proposed antenna's performance has been in-

vestigated with and without the AMC surface, and a gain enhancement of approximately 2.5 dBi and improved radiation efficiency have been attained, as shown in Fig. 6. From this figure, it can be seen that, due to the presence of the AMC surface, a high gain is obtained. In addition, Fig. 7 demonstrates that employing AMC surfaces improves overall efficiency considerably. Moreover, this employment can provide a self-packaged structure that can control the propagation and suppress the radiation leakage. As a result, it will significantly optimize the radiation surrounding the radiating elements. Furthermore, we can clearly see that the sidelobe levels and front-to-back ratios have improved since surface waves are suppressed in the dielectric substrate, as illustrated in Fig. 8. Meanwhile, Fig. 9 shows that the AMC surface drastically reduces the beamwidths in the E-plane over the operating frequency range.

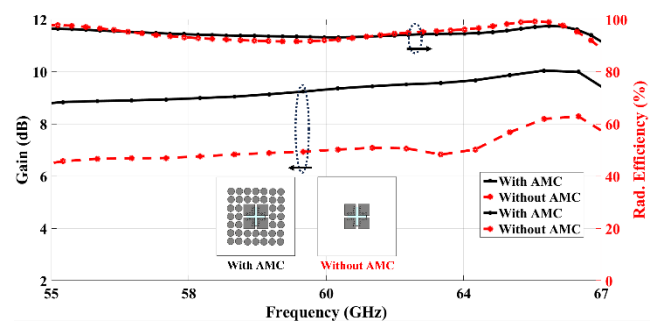


Fig. 6. Simulated gain and efficiency with and without the AMC surface of the presented antenna.

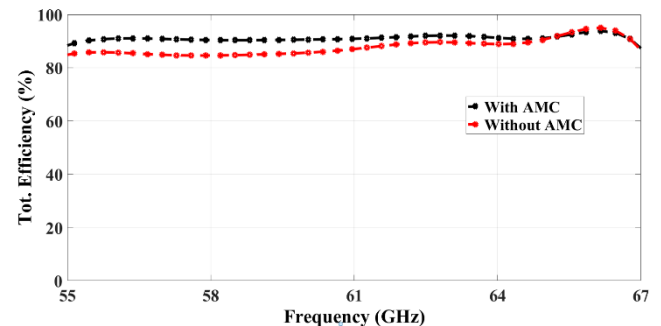


Fig. 7. Simulated total efficiency with and without the AMC surface of the presented antenna.

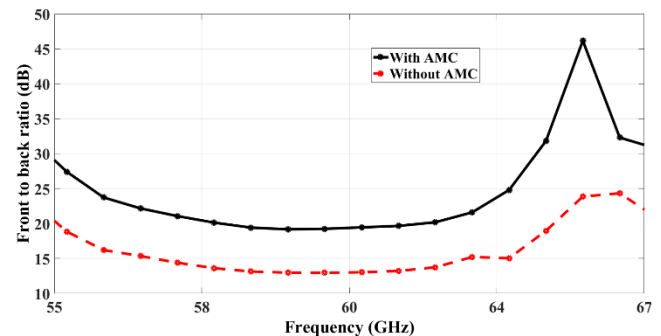


Fig. 8. Simulated front to back ratio of the presented antenna with and without the AMC surface.

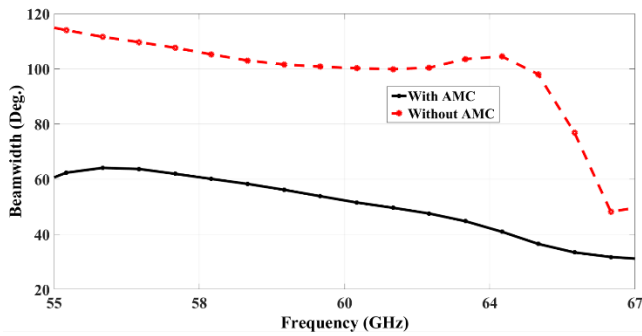


Fig. 9. Simulated 3dB angular beamwidth for the E-plane radiation pattern of the presented antenna with and without the AMC surface.

### III. Head Phantom Model and SAR Calculations

Since many dispersion mechanisms impact human tissues, EM fields are dependent on more than just the strength and frequency of external fields. Furthermore, the body in relation to these external fields depends on its shape, size, and electrical characteristics, as well as its orientation [60]-[62]. The biological effects of the EM field are determined by the amount of absorbed energy and its ability to heat human tissue. Knowing the dielectric properties of biological tissue is necessary to investigate the reflection, transmission, and absorption characteristics of the body. Considering that the magnetic permeability of biological tissues resembles that of free space, electrical permittivity and conductivity are significant aspects of evaluating the EM and power distribution in the body [63]. For the reason human tissues are permeable to RF fields, the RF fields permeate the human tissues when the

body is exposed near the device. The depth of penetration can be determined by the frequency and conductivity of the tissue. For an accurate forecast of the effects of the human body on the propagation and absorption of mm-Wave signals, accurate tissue models should be developed. The simulation setup for the CST head phantom [64] is shown in Fig. 10. Simulations consider the dispersion of electrical properties versus frequency to obtain accurate results [65]. If such is the case, the far-field parameters can be determined based on defining the electrical properties at a center frequency [66]. Due to the fact that most of the mm-wave energy is absorbed within the epidermis and dermis layers of the skin [67], the phantom consists of only the dry skin layer [68]. Thus, the electrical properties at 60 GHz are taken into consideration. The composite of the head model simulating tissue is set with a dielectric permittivity of 7.9753, a loss tangent of 1.3673, a mass density ( $\rho$ ) of 1109 kg/m<sup>3</sup>, and a conductivity of 36.397 S/m [52], [69], [70].

In addition, a truncated head model is used to reduce simulation time. The SAR monitor basically records the losses inside the calculation domain in the form of electric and magnetic losses and uses these losses as a source to compute the SAR distribution in the tissue model.

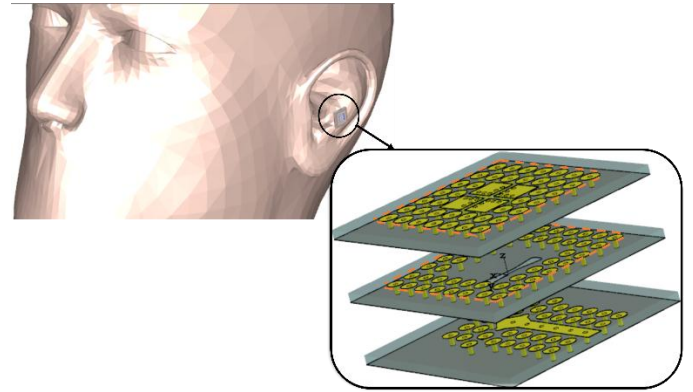


Fig. 10. Simulated model (Head phantom and antenna) with zoomed view of the antenna configuration.

In order to minimize simulation time, it is usual that a simplified head model can be used during simulation. Furthermore, there are several factors that affect absorption, including distance from the radiator, anatomy, orientation of the user, and electrical characteristics of the tissues. Therefore, simulation results are computed at different distances between the radiating source and head model to study the effect of spacing between the radiating source and tissue model, and SAR results for different radiating power are recorded.

The SAR distribution on the human head model of 1 g averaging standard is shown in Fig. 11. Owing to the proposed antenna's wide impedance bandwidth, SAR analysis at multiple operational frequencies has been included. The SAR distribution is calculated assuming that the delivered power to the antenna is 0.1 W. Moreover, at 60 GHz, the SAR is evaluated with transmitting powers of 1 and 10 mW, which are equivalent to those in IEEE Standard 802.15.3-2003 for enabling wireless communications between mobile electronic devices with high-speed, low-power, low-cost multimedia capabilities [71]. Therefore, the SAR values at 60 GHz for different transmitting power levels are recorded in Table 2.

Table 2. SAR values for different transmitting powers at 60 GHz

	Transmitting Power (mW)		
	1 mW	10 mW	100 mW
<b>1g of tissue SAR (W/kg)</b>	0.00451	0.0451	0.451

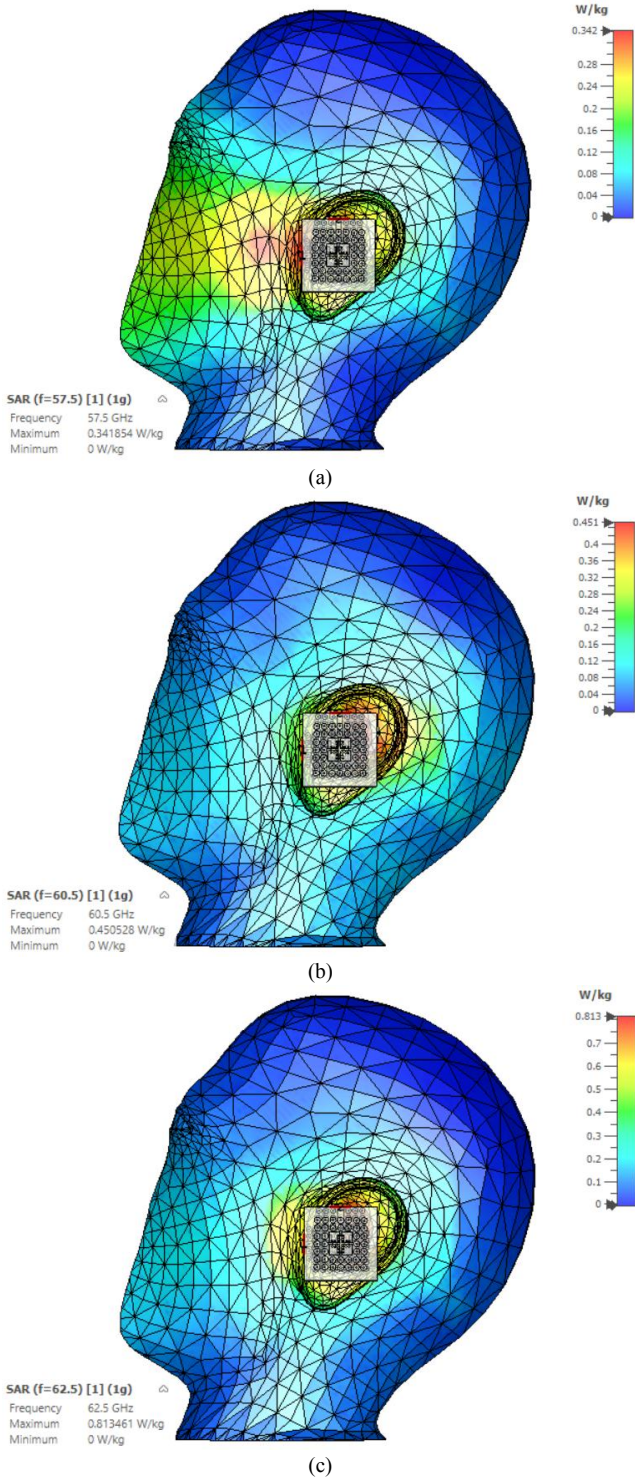


Fig. 11. Simulated head phantom and antenna configuration at different operating frequencies. (a) 57.5 GHz. (b) 60 GHz. (c) 62.5 GHz.

In this study, it was found that the skin depth of radiation decreased at 60 GHz, resulting in hotspots formed as current conduction near the surface. Nevertheless, the impact of hotspots near the source reduces by around 60 GHz due to the substantial attenuation of fields in tissues. In contrast, studies indicate that the distance between the body and the wireless device influences SAR behavior, hence the antenna is kept at a 5mm distance from the body.

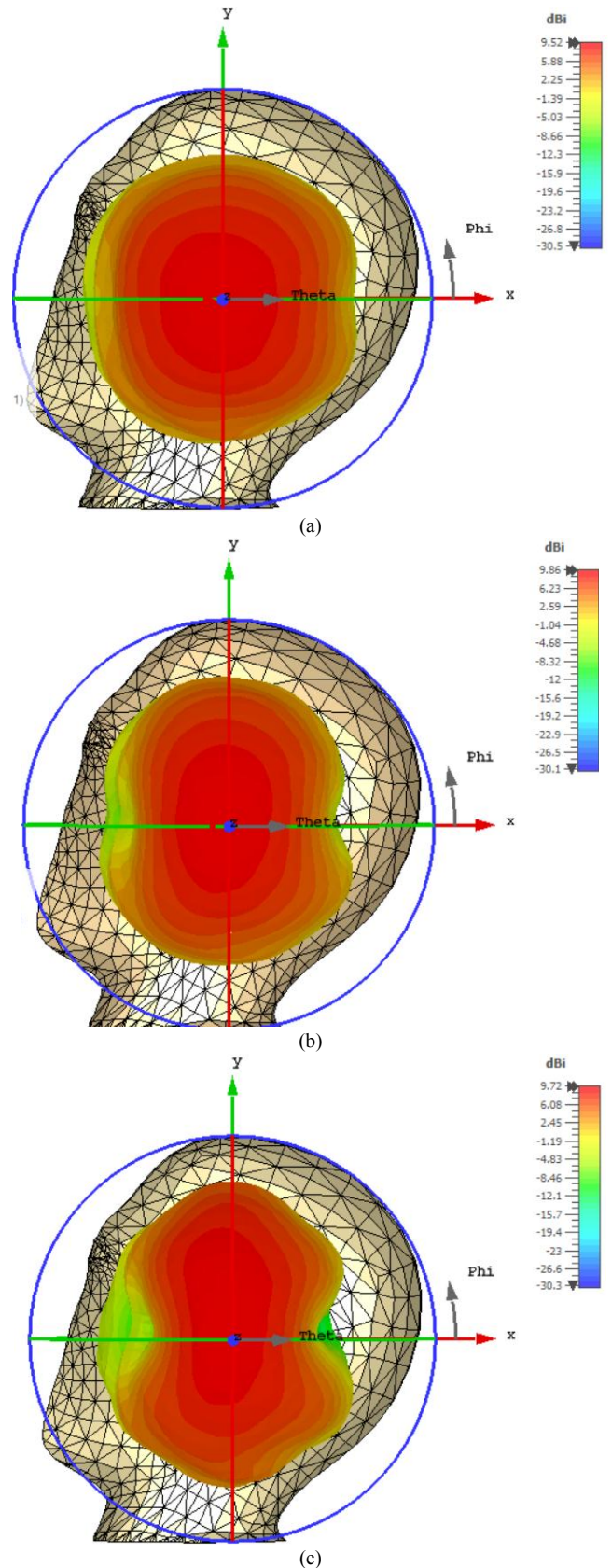


Fig. 12. Simulated head phantom and the associated radiation pattern at different operating frequencies. (a) 57.5 GHz. (b) 60 GHz. (c) 62.5 GHz.

On the other hand, Fig. 12 illustrates the 3D polar patterns for the phantom existence scenario at different operating frequencies. For both free-space and phantom loaded cases,

there are no significant differences between the radiation patterns of free-space and phantom-loaded cases. As a result, the resonance frequency is approximately stable and the radiation pattern remains identical.

For the purpose of evaluating the influence of implementing the AMC surface in the proposed design, the SAR is calculated both with and without the AMC surface. Fig. 13 depicts a brief comparison that demonstrates the considerable contribution made by employing the AMC surface.

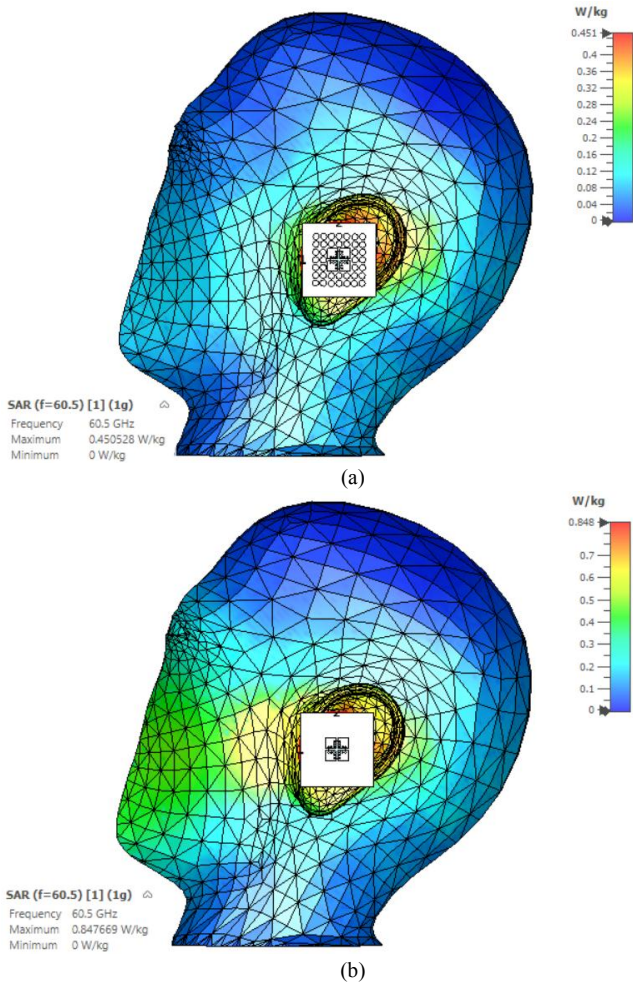


Fig. 13. Simulated head phantom and antenna configuration at 60 GHz. (a) With AMC surface. (b) Without AMC surface.

Table 3. Comparison of SAR 1g averaged values with other technologies at 60 GHz.

Paper	Radiated Power	SAR value 1g Averaged
[52]	100 mW	0.885
[53]	100 mW	1.0442
[72]	100 mW	1.3714
<b>Our work</b>	100 mW	0.451

Our research has identified a limited number of studies on the effect of 60 GHz antennas on the human body. However, the results showed a significant superiority over the other technologies at 60 GHz and were compared with other work in the literature in Table 3. The self-packaged design mostly elim-

inates the effects of dissipation and radiation leakage on the circuit's performance. The PGW technology addresses the rising demand for communication systems in the 60 GHz band.

#### IV. Conclusion

The PGW-based ME-dipole antenna has been demonstrated. The antenna is excited through the square cavity using two PGW lines located at different layers. A cross-shaped slot has been formed on the top ground of the cavity to excite the antenna. The effects of mm-Wave exposure at 60 GHz on human tissue have been investigated. The exposure effects of a human head model are calculated on the basis of SAR and subjected to a radiating source. This study provides substantial evidence for future emerging PGW antenna technology, permitting further development as a potential guiding structure approaches. As a result, PGW technology opens up a wide door for many applications at mm-Wave, especially at 60 GHz, for safe communication systems in the future.

#### REFERENCES

- [1] P. Padilla et al. , "Future 5G Millimeter Wave Systems and Terminals: Propagation Channel, Communication Techniques, Devices, and Measurements," *IEEE Commun. Mag.*, vol. 56, no.7, pp. 12-13, July 2018.
- [2] S M.1457-14 (01/2019)- Detailed specifications of the terrestrial radio interfaces of International Mobile Telecommunications-2000 (IMT-2000).
- [3] Ahmad, I., Ullah, S., Ullah, S., Habib, U., Ahmad, S., Ghaffar, A., ... & Limiti, E. " Design and analysis of a photonic crystal based planar antenna for THz applications," *Electronics*, vol. 10, no. 16, pp. 1941, 2021.
- [4] Khaleel, S. A., Hamad, E. K., Parchin, N. O., & Saleh, M. B. " Programmable beam-steering capabilities based on graphene plasmonic THz MIMO antenna via reconfigurable intelligent surfaces (RIS) for IoT applications," *Electronics*, no. 12, vol. 1, pp. 164, 2022.
- [5] M. M. Abdin, W. Joel, D. Johnson and T. M. Weller, "A system and technology perspective eon future 5G mm-wave communication systems," 2017 IEEE 18<sup>th</sup> Wireless and Microwave Technology Conference (WAMICON), Cocoa Beach, FL, pp.1-6, 2017.
- [6] P. Smulders, "Exploiting the 60 GHz band for local wireless multimedia access: Prospects and future directions," *IEEE Commun. Mag.*, vol. 40, no. 1, pp. 140–147, Jan. 2002.
- [7] T. S. Rappaport, J. N. Murdock, and F. Gutierrez, Jr., "State of the art in 60-GHz integrated circuits and systems for wireless communications," *Proc. IEEE*, vol. 99, no. 8, pp. 1390–1436, Aug. 2011.

- [8] Yilmaz, T., Fadel, E., & Akan, O. B. "Employing 60 GHz ISM band for 5G wireless communications," In IEEE international black sea conference on communications and networking (BlackSeaCom), pp. 77-82, May 2014.
- [9] Al-Yasir, Y. I., Al-Behadili, H. A., Sawadi, B. A., Parchin, N. O., Abdulkhaleq, A. M., Abdullah, A. S., & Abd-Alhameed, R. A. "New Radiation Pattern-Reconfigurable 60-GHz Antenna for 5G Communications," IntechOpen, 2019.
- [10] Ullah, A., Parchin, N. O., Abd-Alhameed, R. A., & Excell, P. S. " Coplanar waveguide antenna with defected ground structure for 5G millimeter wave communications," In 2nd IEEE Middle East and North Africa COMMUNICATIONS Conference (MENACOMM), pp. 1-4, November 2019.
- [11] T. S. Rappaport, G. R. MacCartney, M. K. Samimi and S. Sun, "Wideband Millimeter-Wave Propagation Measurements and Channel Models for Future Wireless Communication System Design," IEEE Trans. Commun., vol. 63, no. 9, pp. 3029-3056, Sept. 2015.
- [12] J. H. van Vleck, "The absorption of microwaves by oxygen," Phys. Rev. J. Arch., vol. 71, no. 7, pp. 413-424, 1947.
- [13] Al-Sadoon, M. A., Patwary, M. N., Zahedi, Y., Parchin, N. O., Aldelemy, A., & Abd-Alhameed, R. A. " A New Beam-forming Approach Using 60 GHz Antenna Arrays for Multi-Beams 5G Applications," Electronics, vol. 11, no. 11, pp.1739, 2022.
- [14] Munir, M. E., Al Harbi, A. G., Kiani, S. H., Marey, M., Parchin, N. O., Khan, J., ... & Abd-Alhameed, R. A. " A new mm-wave antenna array with wideband characteristics for next generation communication systems," Electronics, vol. 11, no. 10, pp. 1560, 2022.
- [15] Ojaroudiparchin, N., Shen, M., & Pedersen, G. F. "  $8 \times 8$  planar phased array antenna with high efficiency and insensitivity properties for 5G mobile base stations," In 10th European conference on antennas and propagation (EuCAP), pp. 1-5, April 2016.
- [16] Luk, K. M., & Wong, H., "A new wideband unidirectional antenna element," Int. j. microw. opt. technol, vol. 1, no. 1, pp. 35-44, 2006.
- [17] Ali, M. M. M., and Sebak, A. R. "2-D scanning magnetoelectric dipole antenna array fed by RGW butler matrix", IEEE Transactions on Antennas and Propagation, Vol. 66, No. 11, PP. 6313-6321, 2018.
- [18] Ng, K. B., Wong, H., So, K. K., Chan, C. H., & Luk, K. M., "60 GHz plated through hole printed magneto-electric dipole antenna," IEEE transactions on antennas and propagation, vol. 60, no. 7, pp. 3129-3136, 2012.
- [19] Luk, K. M., & Li, M., "Magneto-electric dipole antennas for millimeter-wave applications," Asia-Pacific Microwave Conference Proceedings (APMC), pp. 304-306, Nov. 2013.
- [20] Li, M., & Luk, K. M., "Wideband magneto-electric dipole antenna for 60-GHz millimeter-wave communications," IEEE Transactions on Antennas and Propagation, vol. 63, no. 7, pp. 3276-3279, 2015.
- [21] Li, M., & Luk, K. M., "Low-cost wideband microstrip antenna array for 60-GHz applications," IEEE Transactions on Antennas and Propagation, vol. 62, no. 6, pp. 3012-3018, 2014.
- [22] Yang, S. L. S., Kishk, A. A., Lee, K. F., Luk, K. M., & Lai, H. W., "The design of microstrip patch antenna with four polarizations," IEEE Radio and Wireless Symposium, pp. 467-470, Jan., 2008.
- [23] Wang, J., Li, Y., Ge, L., Wang, J., & Luk, K. M., "A 60 GHz horizontally polarized magnetoelectric dipole antenna array with 2-D multibeam endfire radiation," IEEE Transactions on Antennas and Propagation, vol. 65, no. 11, pp. 5837-5845, 2017.
- [24] Zhu, Q., Ng, K. B., Chan, C. H., & Luk, K. M., "Substrate-integrated-waveguide-fed array antenna covering 57-71 GHz band for 5G applications," IEEE Transactions on Antennas and Propagation, vol. 65, no. 12, pp. 6298-6306, 2017.
- [25] P. S. Kildal, E. Alfonso, A. Valero-Nogueira, and E. Rajo-Iglesias, "Local metamaterial-based waveguides in gaps between parallel metal plates," IEEE Antennas and Wireless Propagation Letters, vol. 8, pp. 84-87, 2009.
- [26] P. S. Kildal, "Waveguides and transmission lines in gaps between parallel conducting surfaces," European patent application No. PCT/EP2009/057743, 2009.
- [27] P.-S. Kildal, A. U. Zaman, E. Rajo-Iglesias, E. Alfonso, and A. Valero Nogueira, "Design and experimental verification of ridge gap waveguides in bed of nails for parallel plate mode suppression," IET Microw., Antennas Propag., vol. 5, no. 3, pp. 262-270, Mar. 2011.
- [28] P. S. Kildal, "Three metamaterial-based gap waveguides between parallel metal plates for mm/submm waves," 3rd European Conference on Antennas and Propagation, pp. 28-32, Berlin, Mar. 2009.
- [29] D. Zarifi, A. Farahbakhsh, A. U. Zaman and P. S. Kildal, "Wide-Band Slot Antenna Arrays with Single-Layer Corporate-Feed Network in Ridge Gap Waveguide Technology," IEEE Trans. Antennas Propag., vol. 64, no. 7, pp. 2905-2913, July 2016.
- [30] A. Farahbakhsh, D. Zarifi and A. U. Zaman, "60-GHz Groove Gap Waveguide Based Wideband H-Plane Power Dividers and Transitions: For Use in High-Gain Slot Array Antenna," in IEEE Transactions on Microwave Theory and Techniques, vol. 65, no. 11, pp. 4111-4121, Nov. 2017.
- [31] N. Bayat-Makou and A. A. Kishk, "Realistic Air-Filled TEM Printed Parallel-Plate Waveguide Based on Ridge Gap Waveguide," in IEEE Transactions on Microwave Theory and Techniques, vol. 66, no. 5, pp. 2128-2140, May 2018.
- [32] A. Farahbakhsh, D. Zarifi, A. U. Zaman and P. S. Kildal, "Corporate distribution networks for slot array antenna based on groove gap waveguide

- technology," 2016 10th European Conference on Antennas and Propagation (EuCAP), Davos, pp. 1-3, 2016.
- [33] A. Farahbakhsh, D. Zarifi and A. U. Zaman, "A mmWave Wideband Slot Array Antenna Based on Ridge Gap Waveguide With 30% Bandwidth," in IEEE Transactions on Antennas and Propagation, vol. 66, no. 2, pp. 1008-1013, Feb. 2018.
- [34] H. Raza, J. Yang, P.-S. Kildal, and E. A. Alós, "Microstrip-ridge gap waveguide Study of losses, bends, and transition to WR-15", IEEE Trans. Microw. Theory Techn., vol. 62, no. 9, pp. 1943- 1952, Sep. 2014.
- [35] A. Vosoogh, M. S. Sorkherizi, A. U. Zaman, J. Yang and A. A. Kishk, "An Integrated Ka-Band Diplexer-Antenna Array Module Based on Gap Waveguide Technology With Simple Mechanical Assembly and No Electrical Contact Requirements," in IEEE Transactions on Microwave Theory and Techniques, vol. 66, no. 2, pp. 962-972, Feb. 2018.
- [36] A. U. Zaman and P.-S. Kildal, "Gap waveguides," in Handbook of Antenna Technologies, Z. N. Chen, D. Liu, H. Nakano, X. Qing, and T. Zwick, Eds. Singapore: Springer, 2016, pp. 3273–3347.
- [37] Ali, M. M. M., Shams, S. I., and Sebak, A. R.. "Printed ridge gap waveguide 3-dB coupler: Analysis and design procedure", IEEE Access, Vol. 6, PP. 8501-8509, 2017.
- [38] M. M. M. Ali, S. I. Shams and A. Sebak, "Ultra-wideband printed ridge gap waveguide hybrid directional coupler for millimetre wave applications," IET Microwaves, Antennas and Propagation, vol. 13, no. 8, pp. 1181-1187, 2019.
- [39] M. M. M. Ali and A. Sebak, "Compact Printed Ridge Gap Waveguide Cross over for Future 5G Wireless Communication System," IEEE Microwave Wireless Compon. Lett., vol. 28, no. 7, pp. 549-551, July 2018.
- [40] I. Afifi, M. M. M. Ali and A. Sebak, "Analysis and Design of a Wideband Coaxial Transition to Metal and Printed Ridge Gap Waveguide," IEEE Access, vol. 6, pp. 70698-70706, 2018.
- [41] Ali, M. M. M., Afifi, I., & Sebak, A. R. " A dual-polarized magneto-electric dipole antenna based on printed ridge gap waveguide technology," IEEE Transactions on Antennas and Propagation, vol. 68, no. 11, pp. 7589-7594, 2020.
- [42] Shahzad, M. A., Paracha, K. N., Naseer, S., Ahmad, S., Malik, M., Farhan, M., ... & Sharif, A. B. " An artificial magnetic conductor-backed compact wearable antenna for smart watch iot applications," Electronics, vol. 10, no. 23, pp. 2908, 2021.
- [43] Ahmad, S., Ghaffar, A., Li, X. J., & Cherif, N. " A millimetre-wave tri-band antenna embedded on smart watch for wearable applications," In International Symposium on Antennas and Propagation (ISAP), pp. 1-2. October 2021.
- [44] Michaelson S, ed. "Fundamental and Applied Aspects of Nonionizing Radiation", Springer Science & Business Media. p. xv. ISBN 978-1468407600, 2012.
- [45] Koh, C. The benefits of 60 GHz unlicensed wireless communications. YDI Wireless Whitepaper, 2004.
- [46] IEEE Standard for Safety Levels with Respect to Human Exposure to Radio Frequency Electromagnetic Fields, 3 kHz to 300 GHz, in IEEE Std C95.1-2005, pp.1-238, April 2006.
- [47] International Commission on Non-Ionizing Radiation Protection, Health issues related to the use of hand-held radio telephones and base transmitters, Health Phys., vol. 70, no. 4, pp. 587-593, April 1996.
- [48] Ahmad, S., Paracha, K. N., Sheikh, Y. A., Ghaffar, A., Butt, A. D., Alibakhshikenari, M., ... & Falcone, F. " A metasurface-based single-layered compact AMC-backed dual-band antenna for off-body IoT devices," IEEE Access, vol. 9, pp. 159598-159615, 2021.
- [49] Sheikh, Y. A., Paracha, K. N., Ahmad, S., Bhatti, A. R., Butt, A. D., & Rahim, S. K. A. " Analysis of compact dual-band metamaterial-based patch antenna design for wearable application," Arabian Journal for Science and Engineering, pp. 1-10, 2021.
- [50] Ahmad, S., Manzoor, B., Naseer, S., Ghaffar, A., & Hussein, M. "A Flexible Broadband CPW-Fed Circularly Polarized Biomedical Implantable Antenna With Enhanced Axial Ratio Bandwidth, 2021.
- [51] Ahmad, S., Ghaffar, A., Hussain, N., & Kim, N. " Compact dual-band antenna with paired L-shape slots for on-and off-body wireless communication," Sensors, vol. 21, no. 23, pp. 7953, 2021.
- [52] Hamed, T., Maqsood, M., "SAR Calculation & Temperature Response of Human Body Exposure to Electromagnetic Radiations at 28, 40 and 60 GHz mmWave Frequencies," Progress In Electromagnetics Research, vol. 73, pp. 47-59, 2018.
- [53] Shrivastava, P., Rama Rao, T. "Investigations of SAR distributions and temperature elevation on human body at 60 GHz with corrugated antipodal linear tapered slot antenna," Progress In Electromagnetics Research, vol. 59, pp. 111-121, 2017.
- [54] Guan, J., Yan, S., Jin, J. M. "Electromagnetic simulation of specific absorption rate at 5G frequencies with a simplified human head model and a multi-solver method", IEEE International Symposium on Antennas and Propagation & USNC/URSI National Radio Science Meeting, pp. 941-942, July, 2017.
- [55] Zhu, Q., Ng, K. B., & Chan, C. H. "Complementary source based circularly polarized antenna arrays for millimeter-wave applications," In 2014 IEEE International Workshop on Electromagnetics (iWEM), pp. 260-261, August 2014.
- [56] Clavin, A., Huebner, D., & Kilburg, F. "An improved element for use in array antennas," IEEE Transactions on Antennas and Propagation, vol. 22, no. 4, pp. 521-526, 1974.
- [57] Ali, M. M. M., Al-Hasan, M., Mabrouk, I. B., & Denidni, T. A. " Ultra-wideband hybrid magneto-electric dielectric-resonator dipole antenna Fed by a Printed RGW for Millimeter-Wave Applica-

- tions," IEEE Access, vol. 10, pp. 2028-2036, 2021.
- [58] Mousavirazi, Z., Ali, M. M. M., & Denidni, T. A. "Millimeter-Wave High Gain Hybrid ME-DRD Antenna Fed by PRGW Technology," IEEE International Symposium on Antennas and Propagation and USNC-URSI Radio Science Meeting (AP-S/URSI), pp. 9-10, July 2022.
- [59] Hassan, A. T., & Kishk, A. A. "Efficient procedure to design large finite array and its feeding network with examples of ME-dipole array and microstrip ridge gap waveguide feed," IEEE Transactions on Antennas and Propagation, vol. 68, no. 6, pp. 4560-4570, 2020.
- [60] Halla, P., "Specific absorption rate design of 3rd generation handsets," Mater Dissertation Theses, Helsinki University Of Technology, Finland, 2008.
- [61] Butet, R., Y. Toutain, S. L. Dall, J. Luc, L. J. Foged, and J. Estrada, "A fast SAR measurements system for production testing of personal wireless devices," IEEE Intern. Symp. on Antennas and Prop. Society (APSURSI), pp. 2026–2027, Jul. 2013.
- [62] Zhadobov, M., N. Chahat, R. Sauleau, C. L. Quement, and Y. Le drean, "Millimeter-wave interactions with the human body: State of knowledge and recent advances," Int. Journal of Microwave and Wirel. Tech., vol. 3, no. 2, pp. 237–247, Apr. 2011.
- [63] Alekseev, S. I. and M. C. Ziskin, "Human skin permittivity determined by millimeter wave reflection measurements," Bioelectromagnetic, vol. 28, no. 5, pp. 331–339, 2007.
- [64] CST-Computer Simulation Technology, Documentation, Available on-line at: <http://www.cst.com>, 2020.
- [65] Mahfouz, A. M., Shams, S., Elsaadany, M., & Gagnon, G. "Safety metrics investigation of an electrically coupled patch antenna for sub-6 GHz portable devices serving 5G/6G systems," In IEEE International Symposium on Antennas and Propagation and USNC-URSI Radio Science Meeting (APS/URSI), pp. 599-600, December 2021.
- [66] Abdul-Al, M., Amar, A. S., Elfergani, I., Littlehales, R., Ojaroudi Parchin, N., Al-Yasir, Y., ... & Abd-Alhameed, R. A. "Wireless electromagnetic radiation assessment based on the specific absorption rate (SAR): A review case study. Electronics, vol. 11, no. 4, pp. 511, 2022.
- [67] W. Hong, "Solving the 5G Mobile Antenna Puzzle: Assessing Future Directions for the 5G Mobile Antenna Paradigm Shift," IEEE Microw. Mag., vol. 18, no. 7, pp. 86–102, Nov.-Dec. 2017.
- [68] Bang, J., & Choi, J. "A SAR reduced mm-wave beam-steerable array antenna with dual-mode operation for fully metal-covered 5G cellular handsets," IEEE Antennas and Wireless Propagation Letters, vol. 17, no. 6, pp. 1118-1122, 2018.
- [69] C. Gabriel, "A Compilation of the Dielectric Properties of Body Tissues at RF and Microwave Frequencies," Radiofrequency Radiation Division, Brooks AFB, San Antonio, TX, Contract AL/OE-TR-1996–0037, 1996.
- [70] Dielectric Properties of Body Tissues Institute for Applied Physics, "Nello Carrara" -Florence (Italy), 1987 [Online]. Available: <http://niremf.ifac.cnr.it/tissprop/htmlclie/htmlclie.php>
- [71] Gilb, P. K. J., "Wireless multimedia: A guide to the IEEE 802.15. 3 standard," IEEE Standards Association, 2004.
- [72] Hong, Y., & Choi, J. "60 GHz patch antenna array with parasitic elements for smart glasses," IEEE Antennas and Wireless Propagation Letters, vol. 17, no. 7, pp. 1252-1256, 2018.